Materials Transactions, Vol. 48, No. 5 (2007) pp. 1143 to 1148

EXPRESS REGULAR ARTICLE

Magnetic and Optical Properties of Isolated Magnetite Nanocrystals

Chang-Neng Shauo[1], Chuen-Guang Chao[1,*], Tsien Ming Wu[2] and Hsiou-Jeng Shy[2]

[1]*Department of Materials Science and Engineering, National Chiao Tung University, 1001 Ta Hsueh Road, Hsinchu, Taiwan 300, R. O. China*
[2]*Materials & Electro-Optics Research Division, Chung Shan Institute of Science and Technology, P. O. Box. 90008-8-8, Lung-Tan, Tao-Yuan, 325, Taiwan, R. O. China*

Following preparation of isolated nano-sized magnetite particles in a low-concentration dispersant solution, this study investigated the magnetic and optical properties. Magnetic measurements indicated that the magnetite nanoparticles exhibited perfect superparamagnetism above the blocking temperature. Optical measurements revealed that the magnetic films exhibited good transmittance in the visible region and excellent UVB absorption. It has potential for use in optical applications (UVB-cut), such as sunglasses, heat mirror film and others.
[doi:10.2320/matertrans.48.1143]

(Received February 16, 2007; Accepted March 22, 2007; Published April 25, 2007)

Keywords: *magnetite, nanoparticles, superparamagnetism, blocking temperature, ultraviolet B-cut*

1. Introduction

Nanometer sized magnetite particles, for example, exhibit a size effect. Below a critical size, magnetic particles become single-domain as opposed to multi-domain in the bulk structure. Additionally, small magnetic particles exhibit unique phenomena, such as superparamagnetism and quantum tunneling of magnetization. Furthermore, nanoscale magnetic particles can exhibit unusually high coercities. Nanoscale magnetic particles have great potential for use in such diverse areas as information storage, printing inks,[1,2] magnetic fluids,[3] drugs,[4] biomedical device[5] and magnetic refrigerator[6] because they have unique physical characteristics.

Most studies of nano-sized magnetic particles include ultrafine metallic iron and iron alloy particles,[7] quenched ferrofluid and surfactant-vesicle incorporated magnetite particles,[8] as well as nano-sized iron, iron alloy and iron oxide particles embedded in Al_2O_3, SiO_2[9] and porous glass matrices.[10] Almost all studies, however, have focused only on the magnetic properties of the material.

Rao *et al.* studied the effect of particle sizes on optical transmission through the magnetite fluid with reference to external magnetic fields and incident optical wavelengths.[11] They found that transmittance increases with the magnetic field when the particles are small. However, they did not discuss the optical characteristics of magnetite films in zero field. In this work, isolated nano-sized magnetite particles were prepared in a low-concentration dispersant solution, and the magnetic and optical characteristics were investigated. Experimental magnetization and susceptibility data revealed superparamagnetic behavior above the blocking temperature. Additionally, the optical properties of transparent films that were prepared by magnetite with PU (polyurethane) coated on the glass were studied in zero field. These films exhibit excellent UVB (ultraviolet wavelength ranging from 290–315 nm) absorption and good transmittance in the visible region, suggesting that nano-sized magnetite not only exhibits excellent magnetic properties, but also exhibits favorable optical properties and could be used in optical application.

*Corresponding author, E-mail: c_g_chao@hotmail.com

2. Experimental Methods

2.1 Preparation of magnetite nanocrystals

Highly pure $FeCl_2 \cdot 4H_2O$ (Katayama Chemical), $FeCl_3 \cdot 6H_2O$ and NaOH (Merck) were used. The wetting and dispersing dispersants were commercial grade Disperbyk 181(BYK-Chemie). Deionized water was further purified by distillation (18.2 MΩ).

Magnetite was prepared as follows. 0.15 kmol/m^3 $FeCl_2 \cdot 4H_2O$/0.3 kmol/m^3 $FeCl_3 \cdot 6H_2O$ and three concentrations of the dispersant were dissolved in 400 ml of distilled and deionized water. The concentrations (mass%) of the dispersant were 0, 5.34×10^{-3} and 2.13×10^{-2}. The concentration of the dispersant herein is expressed as mass% which is equivalent to the total amount of composition basis. Table 1 presents the composition of the samples from the dispersing system. 3 kmol/m^3 NaOH aqueous solutions have already been prepared. Then, in the N_2-purged environment, a particular volume of the NaOH solution was dropped into the iron salt solution with vigorous stirring, and the pH of the mixed solution was maintained at pH 11 ± 0.2. When these two solutions were mixed, the system immediately turned black. The reactant was then heated at 80°C for 60 min. The magnetite (plus the bound dispersant) was washed thoroughly three times in deionized water and isolated by magnetic separation from the dissolved dispersant to remove the unbound dispersant. Magnetite particles were thus obtained.

Table 1 Properties of magnetite particles.

Sample	1	2	3
concentration of dispersant (mass%)	0	5.34×10^{-3}	2.13×10^{-2}
Size (nm)	8.2	3.8	1.6
Standard deviation	1.73	1.18	0.51
Saturation magnetization (emu/g)	50.06	45.95	43.95

2.2 Characterization

The size and shape of the magnetite particles were determined by transmission electron microscopy (TEM) and more than 100 particles were observed. Electron micrographs and diffraction patterns were obtained using a JEOL JEM-2010 (at 200 kV) transmission electron microscope. The phase of the powders that had been dried at 70°C in an oven for 24 h was analyzed by powder X-ray diffraction (XRD) using a MAC Science M03X diffractometer at room temperature, with Cu Kα radiation at 40 KV and 20 mA.

Magnetic susceptibility and magnetization were measured using a Quantum Design Model 7-T (MPMS) superconducting quantum interference device (SQUID) magnetometer. Two experiments were performed, determining magnetic susceptibility as a function of temperature and magnetization (M) as a function of field (H) and temperature (T). Two approaches were adopted to measure the dc-magnetic susceptibility. These were (1) zero field cooling (ZFC), in which the sample was slowly cooled in a zero field to a temperature of 2 K, at which a measuring field of 1.0 kG was switched on and magnetization was measured as a function of temperature from 2 to 300 K, and (2) field cooling (FC), in which a field of 1.0 kG was turned on at a temperature that was well above the superparamagnetic blocking temperature before the sample was cooled to 2 K.

Magnetic films, denoted samples F1, F2 and F3, were prepared using three magnetite solutions via spin coating on glass (1.5 cm × 3 cm) followed by drying at 100°C in air for 3 h, to investigate their optical properties. The three magnetite solutions consisted of 5 mass% of magnetite (taken from sample 1,2 and 3, respectively) in 5 mass% of PU and were prepared by adding 5 mass% water-based PU into a suitable amount of colloidal magnetite. The surface morphology and surface distribution of the nanoparticles in the films was studied by atomic force microscopy (HALCYONIC P47). The intensity of transmitted light was measured as a function of incident wavelength on the film between 200 and 800 nm.

3. Results and Discussion

3.1 Particle sizes and structure

The particle sizes of the samples were determined by TEM, as presented in Fig. 1. Table 1 presents their properties. Figure 1 presents the TEM images and histograms [Fig. 1(b) and 1(d)] of these three samples. All of the size distributions were fitted using log-normal laws, and indicated that more dispersant is associated with smaller standard deviation, as described in Table 1, and therefore, a narrower particle size distribution. The structure and composition of the particles were characterized using an electron diffraction pattern [inset of Fig. 1(a)], which demonstrated that the samples comprised magnetite. The image of sample 2 [Fig. 1(a)] reveals that the particles of magnetite that was synthesized at with 5.34×10^{-3} mass% dispersant were relatively uniform in size, and were in the form of isolated spheres. A critical obstacle to assembling and maintaining a nanometer-scale material from molecular clusters is the tendency of such material to aggregate, reducing the energy that is associated with the high surface area-to-volume ratio. However, sample 3 has the highest concentration of added dispersant, resulting from the bridging effect that results in flocculation, as presented in Fig. 1(c). Figure 1(c) shows an undissolved fragment of the dispersant that binds with magnetite particles, because the solubility limit of the dispersant in water is excessive.

Figure 2 plots the variation in the X-ray diffraction patterns with dispersant concentration. The main peaks coincide across all cases. The two most intense diffraction peaks were at $2\theta = 35.55^\circ$ with a d-value of 0.253 nm, and at $2\theta = 62.89^\circ$ with a d-value of 0.1483 nm. The pattern was therefore similar to that produced by the standard Fe_3O_4.

3.2 Magnetic properties

Table 1 presents the properties of magnetite particles. The absolute saturation magnetization fell as the particles size decreased. The specific saturation magnetizations of the particles decreased as the particle size decreased of the fine crystallites (such that the specific surface area increased). The results can be explained using a model of the spin-canted surface layer. The fine crystallites consist of two parts - the surface layer, whose magnetic moment can not be turned completely parallel to the applied field, but can make an average canting angle with the field, and the interior part, whose magnetic moment can be aligned in the direction of the applied field. Based on this assumption, the effect of size on saturation magnetization of fine magnetite particles can be elucidated.[12] Since fine magnetite particles have become fundamental structural units in very-high density-magnetic recording media, the dependence of the specific saturation magnetization on the specific surface area of these fine particles must be studied.

The effect of dispersant on the magnetic properties of Fe_3O_4 nanoparticles is characterized by measurements of the temperature (T)-dependence of the dc susceptibility (χ) and the magnetic field (H)-dependence of the magnetization (M). Figure 3 plots the variation of $\chi(T)$ with temperature for Fe_3O_4 nanoparticles and that of Fe_3O_4 nanoparticles with various concentrations of dispersant. It shows an increase in $\chi(T)$ with T, reaching a maximum value at the blocking temperature (T_b), beyond which it rapidly declines. This behaviour is typical of the superparamagnetic relaxation of nanoparticles. Above T_b, the single-domain magnetic moment of the particles becomes thermally unstable and undergoes superparamagnetic relaxation. Below the blocking temperature, the large magnetic anisotropy causes the particles to become magnetically frozen and to tend to align with the easy axis of magnetization, causing a drop in the magnetic susceptibility as the temperature declines. Notably, sample 1 with large particles has a higher T_b (76.1 K) than the other samples. The blocking temperature increases as the average distance between the particles declines, probably because the strong cluster-cluster interactions become dominant, and are difficult to avoid, because of serious aggregation when is prepared without the use of a dispersant.[13] A previous study in which the blocking temperature increases with particle size has also been confirmed.[14]

Néel and Brown indicated that for particles of volume V, a critical temperature T_b, called the blocking temperature, exists below which the magnetic moment of the particles is fixed, such that their approach to thermodynamic equilibrium

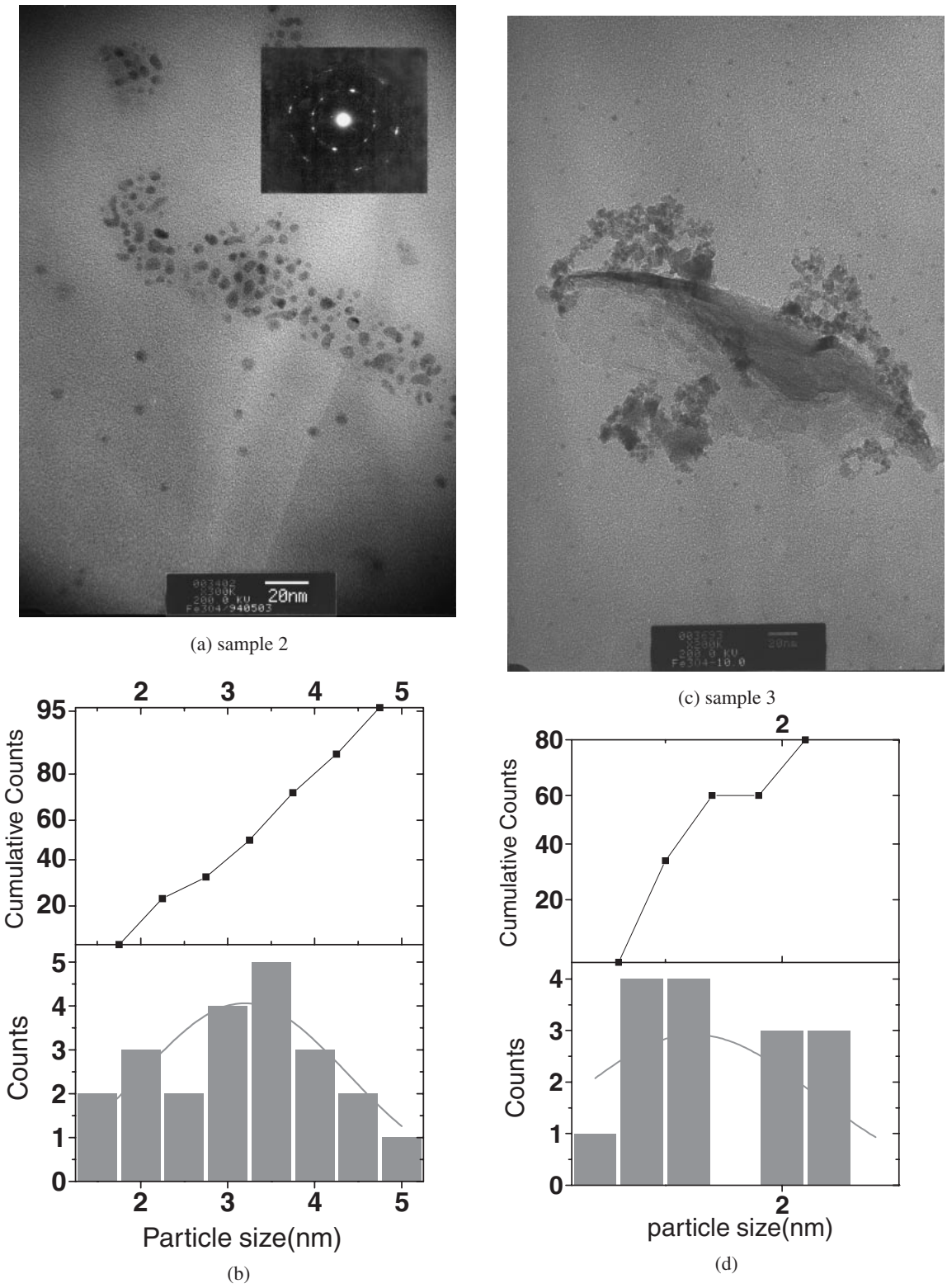

(a) sample 2

(b)

(c) sample 3

(d)

Fig. 1 Transmission electron micrographs and typical particle size distribution of magnetite particles obtained from aqueous solution. The inset of 1(a) shows the electron diffraction pattern. 1(b) and 1(d) are the histograms of sample 2 and 3, respectively.

is blocked. If the time of the experiment is 10^2 s, then the blocking temperature is approximately given by

$$T_b = KV/25k_B \quad (1)$$

where K is the anisotropy energy per unit volume; V is the particle volume, and k_B is Boltzmann's constant. In an assembly of single magnetic domain particles, held at a fixed temperature T, and comprising a distribution of volumes, a critical particle volume V_c, which equals 25 k_BT/K, can be defined, where T corresponds to the blocking temperature of a particle of volume V_c.

At temperatures below the blocking temperature, particles of all sizes smaller than V_c at that temperature and anisotropy are magnetically frozen. Since the magnetic moments are

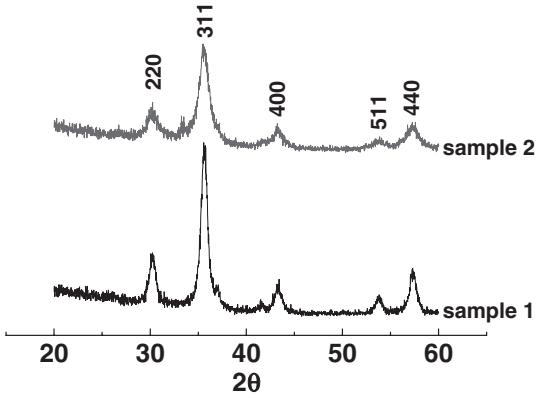

Fig. 2 X-ray diffraction data for samples of Fe_3O_4 obtained from aqueous reactions both with (sample 2) and without (sample 1) dispersant.

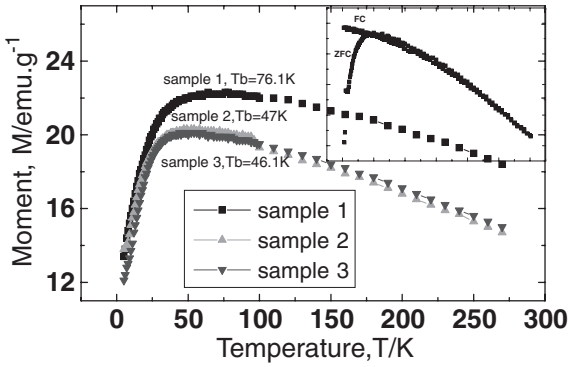

Fig. 3 Plot of dc susceptibility versus temperature of sample 1, 2, and 3.

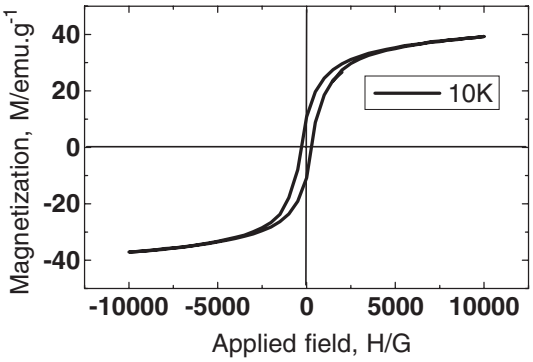

Fig. 4 Magnetization vs. applied field for sample 2 at 10 K.

static, a hysteresis loop will begin to appear in the M(H) curve below the blocking temperature, as presented in Fig. 4. As the external magnetic field increases, the anisotropy barrier declines and the moments follow the field up to saturation. When the field becomes zero, the anisotropy barrier increases to its initial zero-field value. Only the small particles have relaxation times that are comparable to the time-scale of the experiment, such that their magnetic moments return to their thermal equilibrium value by thermal activation or by magnetic tunneling.

The relaxation time, τ, required for the system to reach equilibrium, increases exponentially with KV/k_BT:

$$\tau = \tau_0 \exp(KV/k_BT), \tag{2}$$

where τ_0 is a time constant of the order of 10^{-9} s. τ_0 is related to the rate at which the system attempts to overcome the energy barrier that inhibits thermal equilibrium. In an assembly, the relaxation time of the smaller particles is shorter and, therefore, their response is faster under the influence of an external magnetic field. Larger particles, however, are magnetically frozen and do not respond superparamagneically to the external field. Notably, Equation (2) had to be derived for noninteracting particles. In practice, however, magnetic interactions among particles are commonly significant and may even result in superferromagnetic ordering at low temperatures. This is ordering of the magnetic moments of particles, which would be superparamagnetic if they were isolated.

Superparamagnetic relaxation is important in magnetite nanoparticles. The further development of new high-density magnetic recording media that contain still small magnetic particles may ultimately be limited by superparamagnetic relaxation. A new and interesting application of superparamagnetic particles is in materials for magnetic refrigeration at well above the temperature of liquid helium. Therefore, the subject is of great technological importance.[15)]

The inset in Fig. 3 plots magnetization M as a function of the temperature T in sample 2. The magnetization behaviors of both ZFC and FC samples at temperatures of over 40 K are similar, but change markedly as the temperature declines. The sharp maximum of the ZFC at $T_{max} = 47$ K and splitting between ZFC and FC curves just above T_{max} reveal a narrow particle size distribution.[16)]

3.3 Morphology and optical properties of magnetic films

Figure 5 plots the surface morphology images of the films of samples F2 and F3. The morphology exhibits peaks caused by the magnetite nanoparticles via spin coating with the PU films on the glass and then drying at 100°C in air for 3 h. The average peak height of the film of sample F2 was 4 nm and the average roughness was 0.23 nm. The average peak height of the film of sample F3 was 22.74 nm and the average roughness was 5.35 nm. These results reveal that the magnetite nanoparticles were homogeneously deposited on the glass surface and that the magnetite nanoparticles were well suspended in the PU aqueous media in sample F2. The cross-sectional image in Fig. 5(b) reveals a sharp concavity on the left side, which may result from the shrinking of the sample following drying at 100°C for 3 h. In contrast, sample F1 without added dispersant was too rough to be determined by AFM.

Figure 6 plots transmittance (T) as a function wavelength (λ) for samples F1, F2 and F3. These samples are glass that is coated with approximately 4 μm-thick magnetic films. The transmittance of sample F1 increases markedly from zero to 60% and that of sample F2 from zero to 87%, as the wavelength increases from 200 to 800 nm. Each of the magnetic film samples had a transmission threshold of about 310 nm, while the substrate (glass coated with PU) had a threshold of 270 nm, indicating that sample F2, with excellent roughness [Fig. 5(a)] has better transmittance in the visible region (600–800 nm) than the other samples. All of

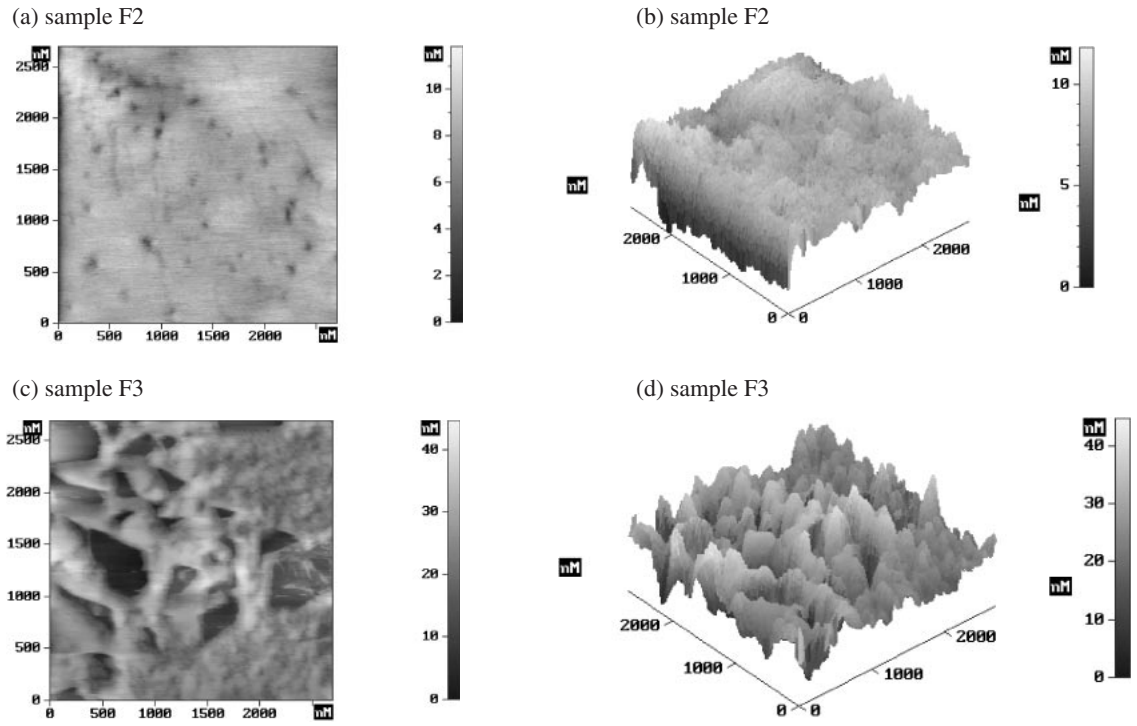

Fig. 5 Surface morphology and three-dimensional surface structure morphology of films of magnetite nanoparticles coated onto glass surface as obtained by atomic force microscopy.

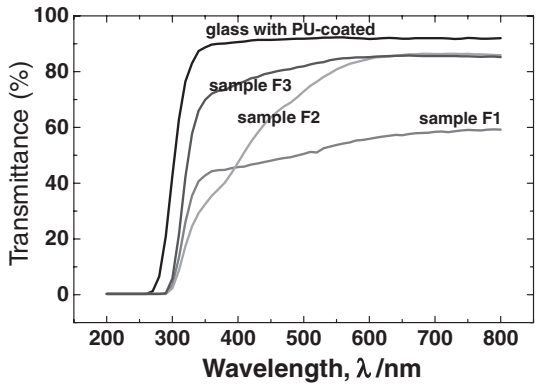

Fig. 6 The variation of the transmittance (T) as a function of wavelength for films of sample F1, F2 and F3. The intensity of transmitted light was measured as a function of incident wavelength between 200 and 800 nm.

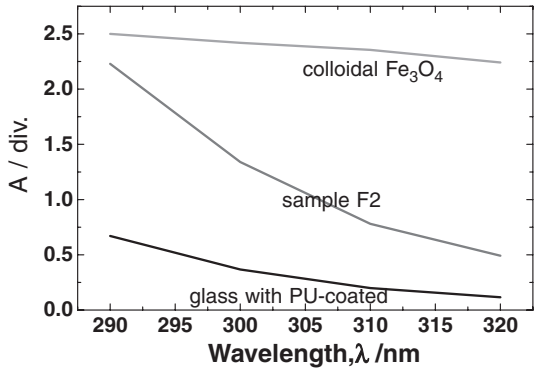

Fig. 7 The variation of the Absorption (A) as a function of wavelength for 5 mass% colloidal Fe_3O_4 (colloidal sample 2), sample F2 and glass with PU-coated. The intensity of transmitted light was measured as a function of incident wavelength between 290 and 320 nm.

the magnetic film samples exhibited a UVB (290–315 nm) cut. Ultraviolet radiation is part of the electromagnetic spectrum that is emitted by the sun. Whereas UVC rays (wavelengths of 100–280 nm) are absorbed by atmospheric ozone, most radiation in the UVA range (315–400 nm) and approximately 10% of the UVB rays (290–315 nm) reach Earth's surface. Both UVA and UVB are very important to human health.[17,18)]

UVB radiation is only partially absorbed by the ozone layer and can damage biological organisms. UVA (wavelengths greater than 320 nm) is not absorbed by ozone and generally does not damage biological organisms. Therefore, UVB protection is critical for human health. This work demonstrated that films of Fe_3O_4 not only can perform UVB-cutting, but also exhibit high transmittance in the visible region. Figure 7 presents the UVB absorption of samples. It reveals that 5 mass% of well-suspended colloidal Fe_3O_4 (sample 2) [Fig. 1(a)] absorbed the most, followed by sample F2. When molecules were irradiated with UV or visible light, electrons in the lowest molecular orbital may be excited and transferred to an orbital of higher energy, increasing the total energy of the molecule and making it unstable. Electron transition in molecules or the absorption of light that is associated with d-d transitions can be explained in terms of this absorption phenomena.[19)] After the molecules absorb photons, they return to their ground states by releasing the absorbed energy to increase stability by relaxation, involving either heat or by light (fluorescence or phosphorescence).

Effective suspension of nano-sized magnetite particles provides more surface area for interaction with UV rays,

resulting in higher absorption. In contrast, the film of sample F2 may have worse absorption because of the particular degree of aggregation that is caused by adding PU, disturbing the absorption. This results reveals that pure nano-sized magnetite is an excellent UVB–cutting material and may have potential optical applications. Possible uses of the binder, however, require further attention. Optical applications depend on high transmittance in the visible region and absorption in the UVB region.

4. Conclusions

Isolated magnetite nanoparticles were synthesized using a dispersing system. The structure and composition of the particles were characterized using an electron diffraction pattern and XRD, which indicated that the samples comprised magnetite. The magnetic measurements revealed that the magnetite nanoparticles exhibited perfect superparamagnetism above the blocking temperature. Optical measurements demonstrated that magnetic films exhibited good transmittance in the visible region and excellent UVB absorption. They can be used in such optical applications as sunglasses and heat mirror films.

Acknowledgement

The authors would also like to thank the National Science Council & Department of Industrial Technology, Ministry of Economic Affairs of the Republic of China, Taiwan, for financially supporting this research under Contract No. NSC95-2221E009-062&95-EC-17-A-08-R7-0706, respectively. Researchers at Chung Shan Institute of Science and Technology is appreciated for performing AFM, TEM and XRD analyses.

REFERENCES

1) T. Atarashi and J. Shimoiizaka: J. Magn. Magn. Mater. **85** (1990) 3–6.
2) Ziolo, US. Patent No. 4474866.
3) I. Nakatani, M. Hijikata and K. Ozawa: J. Magn. Magn. Mater. **122** (1993) 10–14.
4) E. K. Ruuge and A. N. Rusetski: J. Magn. Magn. Mater. **122** (1993) 335–339.
5) S. Roath: J. Magn. Magn. Mater. **122** (1993) 329–334.
6) R. D. McMichael, R. D. Shull, L. J. Swartzendruber and L. H. Bennett: J. Magn. Magn. Mater. **111** (1992) 29–33.
7) Y. Yoshizawa, S. Oguma and K. Yamauchi: J. Appl. Phys. **64** (1988) 6044–6046.
8) W. Luo, S. R. Nagel, T. F. Rosenbaum and R. E. Rosensweig: Phys. Rev. Lett. **67** (1991) 2721–2724.
9) F. H. Liu, M. D. Schultz and M. H. Kryder: J. Appl. Phys. **69** (1991) 5414–5416.
10) N. F. Borelli, D. L. Morse and J. W. H. Schreurs: J. Appl. Phys. **54** (1983) 3344–3350.
11) G. Narsinga Rao, Y. D. Yao, Y. L. Chen, K. T. Wu and J. W. Chen: Phys. Rev. **E72** (2005) 031408.
12) D. H. Han, J. P Wang and H. L. Luo: J. Magn. Magn. Mater. **136** (1994) 176–182.
13) M. EI-Hilo, K. O'Grady and R. W. Chantrell: J. Magn. Magn. Mater. **114** (1992) 295–306.
14) S. Chakrabarti, S. K. Mandal and S. Chaudhuri: Nanotechnology **16** (2005) 506–511.
15) S. Morup and E. Tronc: Phys. Rev. Lett. **72** (1994) 3278–3281.
16) J. K. Vassiliou, V. Mehrotra, M. W. Russell and E. P. Giannelis: J. Appl. Phys. **737** (1993) 5109–5116.
17) http://www.who.int/uv/en/
18) http://uvb.nrel.colostate.edu/
19) A. Schlegel, S. F. Alvarado and P. Wachter: J. Phys. C: Solid State Phys. **12** (1979) 1157–1164.